Bubble entrapment through topological change

S. T. Thoroddsen, K. Takehara, and T. G. Etoh

Citation: Physics of Fluids (1994-present) **22**, 051701 (2010); doi: 10.1063/1.3407654
View online: http://dx.doi.org/10.1063/1.3407654
View Table of Contents: http://scitation.aip.org/content/aip/journal/pof2/22/5?ver=pdfcov
Published by the AIP Publishing

Bubble entrapment through topological change

S. T. Thoroddsen,[1] K. Takehara,[2] and T. G. Etoh[2]
[1]*Division of Physical Sciences and Engineering, King Abdullah University of Science and Technology, Thuwal 23955-6900, Saudi Arabia*
[2]*Civil and Environmental Engineering, Kinki University, Higashi-Osaka 577-8502, Japan*

(Received 8 January 2010; accepted 17 March 2010; published online 3 May 2010)

When a viscous drop impacts onto a solid surface, it entraps a myriad of microbubbles at the interface between liquid and solid. We present direct high-speed video observations of this entrapment. For viscous drops, the tip of the spreading lamella is separated from the surface and levitated on a cushion of air. We show that the primary mechanism for the bubble entrapment is contact between this precursor sheet of liquid with the solid and not air pulled directly through cusps in the contact line. The sheet makes contact with the solid surface, forming a wetted patch, which grows in size, but only entraps a bubble when it meets the advancing contact line. The leading front of this wet patch can also lead to the localized thinning and puncturing of the liquid film producing strong splashing of droplets. © *2010 American Institute of Physics*. [doi:10.1063/1.3407654]

The coating of a solid surface with a layer of liquid is often accomplished with liquid sprays.[1] The uniformity and effectiveness of such coatings are affected by the entrapment of air bubbles under the impacting droplets. The impact of a drop always entraps a bubble under its center,[2–5] principally due to the formation of a stagnation point in the lubricating cushion of air, which deforms the drop, forming a dimple under its center. The rapidly moving lamella can also entrain bubbles through the moving contact line, such as those shown in the still photographs in Fig. 1. Such an entrapment is not observed for millimetric sized water drops, suggesting that the Capillary number ($\mathrm{Ca}=u\mu/\sigma$) at the moving contact line plays a role, as recently suggested by Rein and Delplanque,[6] in addition to the well known splashing parameter $K=\mathrm{Oh}\,\mathrm{Re}^{1.25}$ suggested by Mundo *et al.*[7]

Herein we observe bubble entrapment for drops more than about ten times as viscous as water. We present close-up video images revealing that this entrapment is primarily due to topological changes, which produce new stagnation points in the air flow under the advancing lamella. This occurs when the levitated film makes localized contact with the substrate forming a wet spot, which grows in size to meet the advancing contact line, thus entrapping the bubble, as shown in Fig. 2.

We use gravity-driven water/glycerin drops released from a nozzle 6.1 mm in diameter, generating drops with diameters D around 5.1 mm. The impact velocity U is varied by changing the release heights up to 1.6 m. The Reynolds and Weber numbers of the impact are

$$\mathrm{Re}=\frac{\rho UD}{\mu}\sim 100-2000,\quad \mathrm{We}=\frac{\rho DU^2}{\sigma}\sim 80-2400,$$

where the μ and ρ are the dynamic viscosity and density of the liquid and σ is the surface tension. These parameter values were selected based on our earlier work with Ootsuka *et al.*[8]

To capture the details of the rapid entrapment motions, we use an ultra-high-speed video camera (Shimadzu Hyper-vision, Etoh *et al.*[9]), capable of frame-rates up to 1×10^6 fps, while each video sequence consists of 102 frames, containing 260×312 pixels, irrespective of the frame rate used. The time counter in the accompanying video clips is in microseconds. The drop impacted onto a glass substrate and the spreading was observed through the bottom plate, similar to Thoroddsen *et al.*,[4] using direct lighting from a 350 W metal halide lamp (Sumita MS350). Imaging under the leading edge of the lamella is complicated by the strong curvature of the free surface, making transmitted lighting nonuniform and varying in time.

Figure 1 shows two typical distributions of bubbles entrapped during the impact of a viscous drop. The region around the central bubble[4] (arrowed) is clear, followed by a dense band of bubbles toward the outer edge of the wetted region. Figure 2 shows sketches and close-up observations of the bubble entrapment process. This mechanism requires the formation of a separated tip of the lamella [Fig. 2(a)], which rides on top of a cushion of air.[10] The entrapment occurs when this precursor film makes localized contact with the substrate. Figure 2(d) shows the growth of one such contact region and the resulting entrapment of a bubble, when this

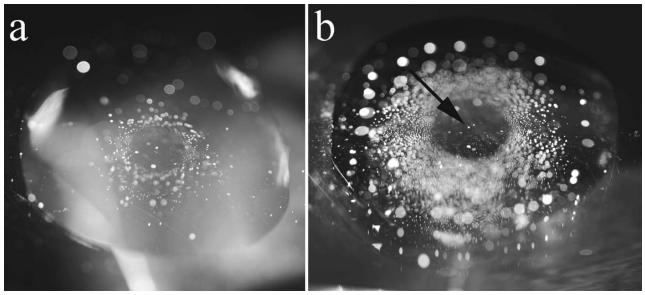

FIG. 1. Myriad of entrapped bubbles under a viscous drop, with 75% glycerin concentration (μ=48 cP) after impacting on a glass plate. (a) Low velocity impact for H=5.1 cm, Re=120, and We=80. (b) Stronger impact for H=19.7 cm, Re=250, and We=350. Photographs are taken after the motions have stopped.

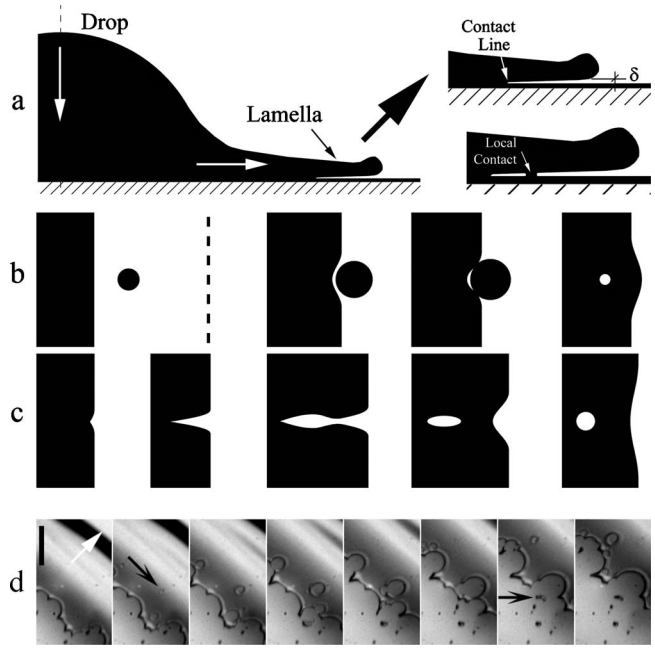

FIG. 2. (a) Sketch of the drop impact, with the lamella moving along the solid substrate and its tip separated riding on a cushion of an air layer of thickness δ. The sketch shows localized contact ahead of the contact line. (b) Top view of the evolution of the localized contact, leading to bubble entrapment. The broken line indicates the tip of the levitating lamella. Dark areas indicate the liquid in contact with the substrate. (c) Different entrapment scenario with a cusp developing in the contact line. (d) Close-up video of the bubble entrapment mechanism, showing contacts of the levitated film with the glass substrate, ahead of the contact line. The light arrow indicates the direction of motion. The first dark arrow points to the onset of one contact and the second to the resulting entrained bubble. For 75% glycerin, Re=570 and Oh=0.090. The bar is 200 μm long. The frames are spaced by 16 μs (enhanced online). [URL: http://dx.doi.org/10.1063/1.3407654.1]

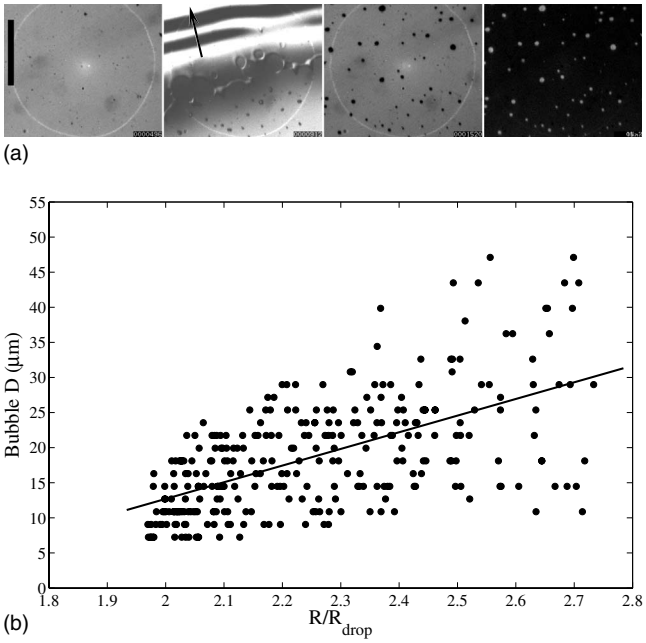

FIG. 3. The bubble size distribution. (a) The last frame is the intensity difference between the frames taken before (first frame) and after (third frame) the front moves across the field of view in the second frame. The scale bar is 500 μm. (b) Diameters of entrapped bubbles vs distance from the impact center, showing all bubbles in a 22° slice of the wetted region, which, when extrapolated, gives a total of 4840 entrapped bubbles. For 75% glycerin (μ=44 cP), H=108 cm, Re=560, and Oh=0.098.

growing contact meets the advancing contact line, as sketched in Fig. 2(b).

The radial growth of the localized circular contact was measured directly from the high-speed video images, showing that $dr/dt=1.2\pm0.2$ m/s, giving a local Ca=0.8. This large spreading velocity, for the partly wetting conditions,[11] suggest that the air layer is very thin to counteract the azimuthal curvature, i.e., $\delta<r$.

The overall view in Fig. 1(b) shows that the bubble size tends to increase with distance from the impact center. This is due to the thickening of the air cushion, through the growth of boundary layers in the air pushed ahead of the contact line along the substrate. The bubble sizes were measured from close-up images, such as those shown in Fig. 3(a). Their diameters are, in this case, between 5 and 50 μm, with the average size growing linearly with the radial distance, as shown in Fig. 3(b).

Figure 4 shows the extent of the bubble entrapment regions for fixed Ohnesorge number $\mathrm{Oh}=\mu/\sqrt{\sigma(D/2)\rho}$, while Re is varied over a range of values. The most robust entrainment occurs for intermediate values of Re, as those shown in Fig. 1(b), where entrapped bubbles extend over a large fraction of the wetted footprint. The largest extent occurs here for $\mathrm{Re}\sim250-350$.

For low impact Re, the levitated sheet remains intact during the spreading and is pulled back into one wetted region (Fig. 1). However, for larger Re, this sheet breaks up in the air, shedding droplets. The localized contacts of the sheet to the substrate, not only control the air entrapment, but also greatly affect the breakup of the levitated sheet into droplets. For an intermediate range of impact velocities, the tip of the lamella thickens and develops Rayleigh instability, shedding isolated droplets, as shown in Fig. 5(a), before being pulled back toward the contact line, often leaving random ligaments along the solid surface. For higher impact Re, the levitated sheet ruptures near the contact line sending off a spray of droplets. The original puncture of the sheet next to the contact line, shown in Fig. 5(b), is clearly promoted by localized attachment. For this Oh=0.028, the transition between these

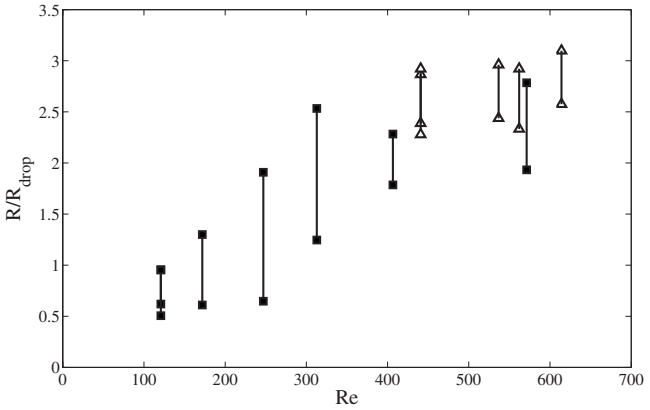

FIG. 4. Radial extent of entrapped bubbles vs impact Re. For 75% glycerin (■) (μ=44 cP), Oh=0.098 and for 80% glycerin (△) ($\mu\simeq$60 cP), Oh =0.135.

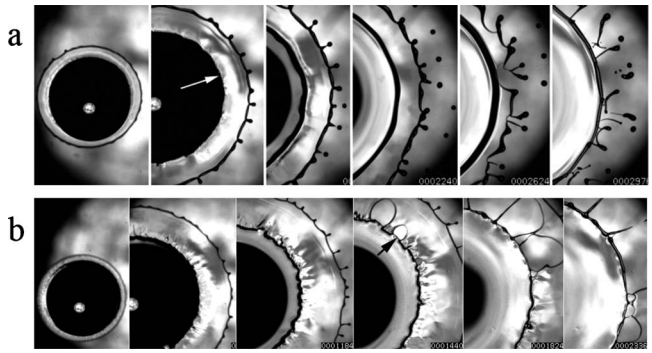

FIG. 5. The transition between different breakup mechanisms of the detached lamella, for 60% glycerin drop (μ=12.2 cP) of D=5.2 mm, Oh =0.028. (a) The front is pulled back toward the center for H=25.3 cm (Re=1060) at t=0.42, 1.22, 1.8, 2.6, 3.0, and 3.3 ms after impact. The arrow points at the contact line. (b) The front is detached from the contact line, promoted by ruptures at localized contacts. Frames shown at t=0.22, 0.67, 0.96, 1.2, 1.6, and 2.1 ms after impact, for H=99.3 cm (Re=2030). The arrow points to a rupture of the liquid sheet (enhanced online). [URL: http://dx.doi.org/10.1063/1.3407654.2] [URL: http://dx.doi.org/10.1063/1.3407654.3]

two outcomes, i.e., pullback of the lamellar edge or the rupture of the film close to the contact line, occurs for Re $\simeq$1500. Note that almost no bubbles are entrained in the case where the front is pulled back in Fig. 5(a). Note that this corresponds to a value of the splashing parameter $K \simeq 30$, which is of the same order as the critical value of 58 found by Mundo *et al.*[7]

Figures 6 shows details of the sheet rupture following the localized contact far ahead of the moving contact line. The sequence in Fig. 6(a) shows three such contacts and rupture of the sheet from two of them. Figure 6(b) shows the characteristic two-lobe *rabbit-ear* structure of these contact regions, which subsequently ruptures slingshotting the sheet forward. The rupture develops first at the contact line on the downstream tip of the contact, marked by an arrow in Fig. 6(a). The sideways ripping speed is ~15 m/s, but keep in mind that this is simply a kinematic point, like the cutting point of scissors. We also note that each contact in Fig. 6(a) entrains a large bubble, as it meets the contact line.

The holes in the liquid sheet grow rapidly in all directions, pulled by surface tension. Where two edges meet they pirouette and often touch the substrate, leaving wet stripes, as can be seen in the last frame of Fig. 5(b).

It remains to be determined what initiates the contact between the levitated film and the substrate. Even though we used a new microscope slide for every impact, the experiments were carried out in a typical civil engineering laboratory without specific dust control. We therefore expect that some microscopic dust or aerosol particles are present on the solid and will promote some of the observed reconnections. However, we believe the susceptibility of the flow to these contacts are intrinsic to this flow geometry. This is supported by the close-up video images accompanying Fig. 2 where the reconnections do not, in general, appear to be associated with any visible dust particles on the plate. One can also imagine that the moving contact line can lead to charge separation and thereby promote reconnections by electrostatic forces.

Some of the contacts could be promoted by slight roughness elements on the solid surface. However, we believe that this roughness is not necessary for this mechanism to occur, as we have verified using optical glass, i.e., one face of a high-quality prism.

We also point out that the free surface gliding ahead of the contact line looks smooth for the lower Re, only for the largest Re in Fig. 5(b), are clear wavelike disturbances present on the sheet surface, perhaps promoted by the uneven advancing contact line, in effect being a self-sustaining process.

It has recently been suggested that air entrainment through the contact line controls splashing and fingering during drop impacts,[6] which would suggest a critical value of

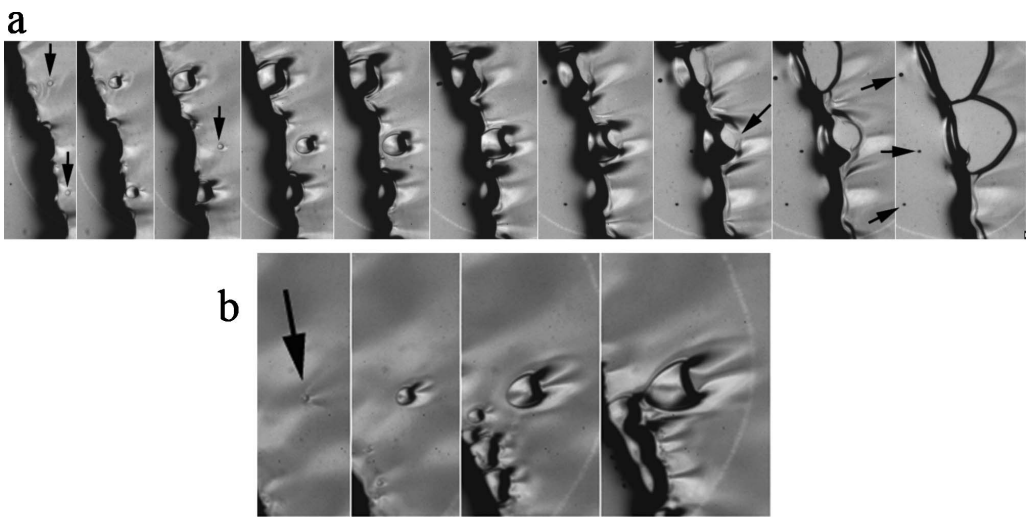

FIG. 6. (a) Three contacts between the lamella and the solid glass plate. Two contacts in the first frame and one contact in the third. Three entrapped bubbles are clear in the last frame. Frames are not evenly spaced, but taken from a 125 kfps video sequence. The arrow in the third to last frame pinpoints the starting point of the rupture, which travels sideways along the contact line. (b) The onset of an isolated contact between the lamella and the solid glass plate. Times shown are t=48, 128, and 208 μs after the first frame (enhanced online). [URL: http://dx.doi.org/10.1063/1.3407654.4] [URL: http://dx.doi.org/10.1063/1.3407654.5]

the local Capillary number $\mathrm{Ca}_{cr}=(dR/dt)\sigma/\mu \simeq 0.25$, based on coating experiments.[12] However, as pointed out by Rein *et al.*,[6] this critical value is not observed for drop impacts. In the experiments of Thoroddsen *et al.*,[4] the region outside the central entrapped bubble, is clear of entrained bubbles, even for $\mathrm{Ca} > 10$. Furthermore, this criterion is not consistent with the fact that the center under the drop is clear of bubbles, in spite of the contact line velocity being highest in this region, immediately following the first contact.

Our observations suggest that the relevant criterion for air entrapment is therefore the stability of the levitated front and not the Ca of the moving contact line. In other words, the entrainment process is a fundamentally three-dimensional and not the usual two-dimensional model used at the contact line or cusps at a free surface.[13] Future work could investigate the relevance of this process to the suppression of splashing in reduced air pressure[14] and the effects of roughness.[15]

In this letter, we investigate the mechanism of air entrapment under an impacting viscous drop, highlighting the role of localized contacts of the levitated lamella with the solid substrate. These contacts change the topology of the air flow entrapping microbubbles and can promote the rupture and splashing of droplets.

[1] K. Shinoda, H. Murakami, S. Kuroda, S. Oki, K. Takehara, and T. G. Etoh, "In situ visualization of impacting phenomena of plasma-sprayed zirconia: From single splat to coating formation," Appl. Phys. Lett. **90**, 194103 (2007).
[2] S. Chandra and C. T. Avedisian, "On the collision of a droplet with a solid surface," Proc. R. Soc. London, Ser. A **432**, 13 (1991).
[3] S. T. Thoroddsen and J. Sakakibara, "Evolution of the fingering pattern of an impacting drop," Phys. Fluids **10**, 1359 (1998).
[4] S. T. Thoroddsen, T. G. Etoh, K. Takehara, K. N. Ootsuka, and Y. Hatsuki, "The air bubble entrapped under a drop impacting on a solid surface," J. Fluid Mech. **545**, 203 (2005).
[5] M. Mani, S. Mandre, and M. P. Brenner, "Events before droplet splashing on a solid surface," J. Fluid Mech. **647**, 163 (2010).
[6] M. Rein and J.-P. Delplanque, "The role of air entrainment on the outcome of drop impact on a solid surface," Acta Mech. **201**, 105 (2008).
[7] C. Mundo, M. Sommerfeld, and C. Tropea, "Droplet-wall collisions: Experimental studies of the deformation and breakup process," Int. J. Multiphase Flow **21**, 151 (1995).
[8] N. Ootsuka, T. G. Etoh, K. Takehara, S. Oki, Y. Takano, Y. Hatsuki, and S. T. Thoroddsen, "Air-bubble entrapment due to a drop," Proc. SPIE **5580**, 153 (2005).
[9] T. G. Etoh, D. Poggemann, G. Kreider, H. Mutoh, A. Theuwissen, A. Ruckelshausen, Y. Kondo, H. Maruno, K. Takubo, H. Soya, K. Takehara, T. Okinaka, and Y. Takano, "An image sensor which captures 100 consecutive frames at 1 000 000 frames/s," IEEE Trans. Electron Devices **50**, 144 (2003).
[10] R. D. Schroll, C. Josserand, S. Zaleski, and W. W. Zhang, "Impact of a viscous liquid drop," Phys. Rev. Lett. **104**, 034504 (2010).
[11] J. C. Bird, S. Mandre, and H. Stone, "Short-time dynamics of partial wetting," Phys. Rev. Lett. **100**, 234501 (2008).
[12] S. F. Kistler, in *Wettability*, edited by J. C. Berg, (Dekker, New York, 1993), pp. 311–349.
[13] J. Eggers, "Air entrainment through free-surface cusps," Phys. Rev. Lett. **86**, 4290 (2001).
[14] L. Xu, W. W. Zhang, and S. R. Nagel, "Drop splashing on a dry smooth surface," Phys. Rev. Lett. **94**, 184505 (2005).
[15] L. Xu, L. Barcos, and S. R. Nagel, "Splashing of liquids: Interplay of surface roughness with surrounding gas," Phys. Rev. E **76**, 066311 (2007).